

DENSITY FLUCTUATIONS, PHASE SEPARATION AND MICROSEGREGATION IN SILICATE GLASSES*

G. N. Greaves, Y. Vaills^a, S. Sen, R. Winter

Department of Physics, University of Wales, Aberystwyth, SY23 3BZ, UK

^aCRMHT, 45071, Orléans, Cedex 2, France

Microstructure in silicate glasses is reviewed from the standpoint of density fluctuations, phase separation and microsegregation. Recent experiments in Brillouin Scattering and Nuclear Magnetic Resonance (NMR) spin relaxation are used to characterise the length scale, magnitude and dimensionality of density fluctuations in monophasic silicate glasses and of phase separation in biphasic glasses. New Small Angle X-ray Scattering (SAXS) experiments are introduced which reveal the presence of much finer microstructure whose geometry is linked with the position and width of the First Sharp Diffraction Peak. For silica this structure resembles the quasiperiodicity recently identified in large tetrahedral model networks. For silicate glasses quasiperiodic order with a shorter spacing occurs in the microsegregation of glass modifiers from glass formers evident from Molecular Dynamic structures as well as from the empirically determined local structure.

(Received October 20, 2000; accepted November 15, 2000)

Keywords: Density fluctuations, Phase separation, Glass structure

1. Introduction

Heterogeneity in glass structure has been known about for more than 60 years but has developed somewhat independently of the modelling of glass structure, which is generally assumed to be homogeneous. This division of labour and of vision has arisen mainly because the techniques that are sensitive to fluctuations in glass density and composition – light scattering, small angle X-ray scattering (SAXS), electron microscopy - are rather distinct from those that are appropriate for probing local atomic structure – neutron scattering, X-ray absorption fine structure (XAFS) spectroscopy, NMR. Nevertheless, with recent improvements in all of these experimental techniques and with the increasing possibilities opening up by computer simulation, it is now possible to look in both directions at once and to endeavour to establish links between microstructure and local structure. Assuredly, more than for any other type of material, the structure of glass is unified across all length scales and this overview attempts to take advantage of this outlook.

2. Density fluctuations

To a first approximation, glass structure has indeed often been regarded as homogeneous. The popular Zachariasen model [1], supported by early X-ray experiments by Warren [2], concluded that glass structure is “an unbroken system of bonding which does not allow any boundaries or voids to produce density fluctuations on a 5 – 50 Å scale”. Where such a Continuous Random Network (CRN) representing a glass former would necessarily depart from a homogeneity on the atomic scale, changes in density at this level were considered by Zachariasen and Warren to be random and hence

* Plenary Lecture at Romanian Conference on Advanced Materials, Bucharest, Romania, October 23-25, 2000

the overall inhomogeneity stochastic. However, in the liquid state single component systems are physically inhomogeneous, the average density ρ_0 , being broken up by thermal fluctuations of mean square density $\langle \Delta\rho^2 \rangle$ given by

$$V\langle \Delta\rho^2 \rangle / \rho_0^2 = k_B T K_T \quad (1)$$

where T is the temperature, V is the volume of the fluctuating elements and K_T is the isothermal compressibility [3]. For the case of viscoelastic liquids $k_B T K_T$ in Eq. (1) can be separated out into

$$k_B T K_T = k_B T (K_T - K_S) + k_B T K_S = k_B T (K_T - K_S) + k_B T K_S^r + k_B T K_S^\infty$$

where $k_B T (K_T - K_S)$ is due to entropy fluctuations at constant pressure, $k_B T K_S^\infty$ relates to fluctuations stemming from the high frequency adiabatic compressibility and $k_B T K_S^r$ to fluctuations related to the complementary relaxation compressibility ($K_S^r = K_S - K_S^\infty$) [4]. Moreover, the high frequency adiabatic compressibility, K_S^∞ , equals $1/(\rho_0 v_\infty^2)$, where v_∞ is the velocity of sound for acoustic vibration modes. Accordingly, as a viscoelastic liquid is cooled, the contribution of $k_B T K_S^\infty$ to $V\langle \Delta\rho^2 \rangle / \rho_0^2$ continues to fall with temperature whilst the remainder, $k_B T_f (K_T - K_S) + k_B T_f K_S^r$, becomes frozen in as density fluctuations as the fictive temperature, T_f , is passed and a glass is formed, i.e.

$$V\langle \Delta\rho^2 \rangle / \rho_0^2 = k_B T_f (K_T - K_S + K_S^r) + k_B T / (\rho_0 v_\infty^2) \quad (2)$$

Given the presence of density fluctuations, $\langle \Delta\rho^2 \rangle$, in a single component material, light or X-rays will be scattered in proportion to $\langle \Delta\rho^2 \rangle$. For light scattering from a glass, the static (Rayleigh) and phonon (Brillouin) contributions to $V\langle \Delta\rho^2 \rangle / \rho_0^2$ are spectroscopically separated [5]. Rayleigh scattering occurs at the frequency of the incident light, ν_0 , and Brillouin scattering at ν , where

$$\nu = 2^{1/2} n v_\infty \nu_0 / c$$

n is being the refractive index. The ratio of the Rayleigh and Brillouin components, called the Landau-Placzek ratio, R_{LP} , is given by

$$R_{LP} = (T_f / T) (\rho_0 v_\infty^2 K_T - 1) \quad (3)$$

where the value for SiO₂ glass at room temperature, for example, is 23 [6]. Eq. (2) and Eq. (3) give

$$V\langle \Delta\rho^2 \rangle / \rho_0^2 = (1 + R_{LP}) k_B T / (\rho_0 v_\infty^2) \quad (4)$$

From the measured R_{LP} values, $V\langle \Delta\rho^2 \rangle / \rho_0^2$ in SiO₂ glass is 1.3 \AA^3 and in B₂O₃ glass a little larger, viz. 2.7 \AA^3 [7].

For (Na₂O)_x(SiO₂)_{1-x} glasses smaller R_{LP} values of around 10 compared to 23 in silica have been measured by one of us (YV) [8], with similar values reported for (K₂O)_x(SiO₂)_{1-x} glasses [9] - in both cases for trisilicate compositions and above ($x \geq 0.25$). Considering Eq. (3), these values for silicate glasses should not be too surprising, as the differences in the corresponding isothermal compressibilities, K_T , between silicate glasses and silica are $< 10 \%$ [8] whereas the fictive temperatures, T_f , for alkali silicates ($x \geq 0.25$) are typically a half those of silica. Also the longitudinal acoustic sound velocities, v_∞ , are smaller. From Eq. (4), the magnitude of density fluctuations, $[\langle \Delta\rho^2 \rangle / \rho_0^2]^{1/2}$, in monophasic silicate glasses might well be lower than in silica. However, in order to establish values for $[\langle \Delta\rho^2 \rangle / \rho_0^2]^{1/2}$ in silica and silicate glasses, estimates are required for the size of the fluctuating volume elements, V .

Density fluctuations in glasses have also been studied by SAXS [10,11]. As X-rays are scattered by fluctuations in electron density, the relevant parameters are ρ_e , the mean electron density, and $\langle \Delta\rho_e^2 \rangle$, the mean square fluctuation in ρ_e , where

$$\langle \Delta\rho_e^2 \rangle / \rho_e^2 = \langle \Delta\rho_0^2 \rangle / \rho_0^2 \quad (5)$$

In particular, at zero scattering angle, the X-ray scattering intensity, I_0 , is given by [12]

$$I_0 = I_e N V^2 \langle \Delta\rho_e^2 \rangle \quad (6)$$

where N is the number of scattering particles and I_e is the X-ray intensity scattered by an electron. This can be rewritten in terms of electron units (e.u.'s) as

$$I_0 = (V\langle\Delta\rho^2\rangle/\rho_0^2) N_A \rho_0 \Sigma Z/M \quad (7)$$

where N_A is Avogadro's number, ΣZ is the number of electrons per scattering unit and M is the molecular weight. Values of I_0 for silica are around 24 e.u.'s [10] and close to 50 for vitreous GeO_2 [11] and B_2O_3 [13].

Comparing Eq. 7 with Eq. 4, it is clear that I_0 gives an independent measure of $(V\langle\Delta\rho^2\rangle/\rho_0^2)$ and taken so in conjunction with the Landau-Placzek ratio, R_{LP} , the magnitude of density fluctuations, $[\langle\Delta\rho^2\rangle/\rho_0^2]^{1/2}$, and their size, $V^{1/3}$, can be determined. For silica $[\langle\Delta\rho^2\rangle/\rho_0^2]^{1/2} \sim 1\%$ and the corresponding volume element is $\sim 8000 \text{ \AA}^3$, equivalent to a 20 \AA cube [14]. Considering the smaller values of R_{LP} in alkali silicate glasses beyond the trisilicate composition, the magnitude of density fluctuations in these binary glasses might indeed be less than in silica [9], but without complementary I_0 SAXS values this has yet to be confirmed.

3. Phase separation

Despite the interest in density fluctuations, microstructure in oxide glasses is, perhaps, best known in the context of compositional fluctuations or phase separation. A two-component mixture may originate in the melt and be quenched into the glass at T_f or be generated from a rapidly quenched homogeneous glass by annealing above the glass transition [14,15,16]. Phase separation in glasses is confined to particular systems and compositions. For example sodium silicate glasses, $(\text{Na}_2\text{O})_x(\text{SiO}_2)_{1-x}$, with compositions above trisilicate ($x \geq 0.25$) are perfectly homogeneous, that is apart from density fluctuations. However for compositions below tetrasilicate ($x \leq 0.2$), the structure bifurcates into regions where the modifier content is less than x and regions where this is greater than x .

Phase separation is conventionally measured using light scattering and electron microscopy, the composition being determined from electron microprobe measurements. Phase diagrams are available for lithium and sodium silicates [17] and some other melts and glasses. Fig. 1 shows the well-known coexistence curve for the $(\text{Na}_2\text{O})_x(\text{SiO}_2)_{1-x}$ system [18], where the separation of soda-rich from silica-rich phases stretches from the liquidus at $845 \text{ }^\circ\text{C}$ down in temperature and covers a composition range approximately given by $0.02 < x < 0.2$. It is asymmetric and peaks around $x = 0.08$. The immiscibility dome is broader in the case of lithium silicates [17] and possibly narrower for potassium silicates [4].

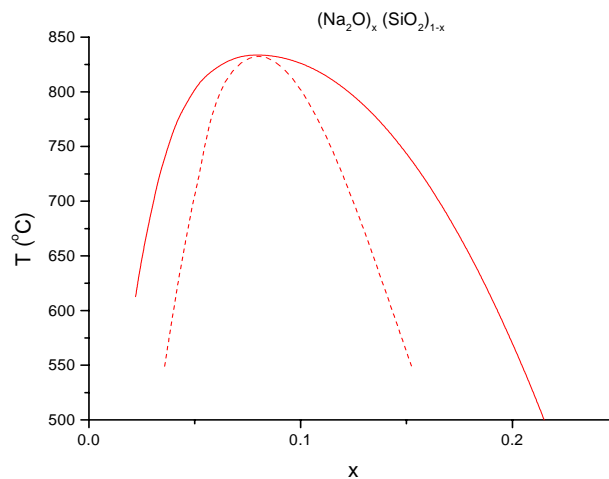


Fig. 1. Sub-liquidus coexistence curve for the $(\text{Na}_2\text{O})_x(\text{SiO}_2)_{1-x}$ system [from 18]. The spinodal, defined by $d^2F/dx^2 = 0$, where F is the free energy, is indicated by the dotted curve. This distinguishes the region of spinodal decomposition in the centre from nucleation and

growth on the flanks.

Phase separation is usually manifest on micron length scales and leads to opal glasses [14] – each phase exhibiting strong connectivity. This is illustrated in Fig. 2 for a $\text{Na}_2\text{O} - \text{SiO}_2$ glass. Phase separation can also be present on a much finer scale in an otherwise transparent glass from which opalescence can be developed by ripening processes. Immiscibility within the coexistence composition range is believed to stem from much smaller fluctuations in composition, x , accompanied by variations in the free energy, F . Thermodynamically phase separation is considered to develop, either by nucleation and growth where F is in the vicinity of a compositional minimum ($d^2F/dx^2 > 0$) [19], or by spinodal decomposition where F falls at a compositional maximum ($d^2F/dx^2 < 0$) [20]. The spinodal, defined by $d^2F/dx^2 = 0$, differentiates between the two regimes. To a first approximation phase separation in the centre of the coexistence region in alkali silicates, for instance, should develop by spinodal decomposition and by nucleation and growth on its flanks. These are differentiated in Fig. 1 by the dotted curve [18]. Morphologically there is little to distinguish qualitatively between the two mechanisms, both spinodal decomposition and nucleation and growth resulting in phase connectivity [21,22]. Quantitatively, though, there may well be geometrical differences, depending on the growth mechanism.

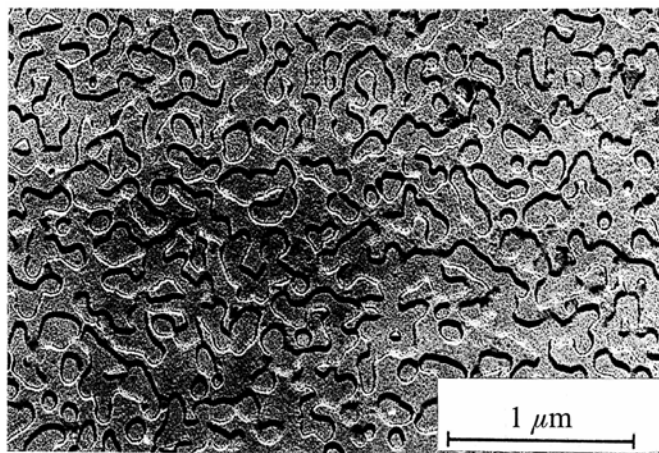


Fig. 2. Fully developed phase separation in a $\text{Na}_2\text{O} - \text{SiO}_2$ glass [16]. Electron micrograph of an etched surface.

Time dependent SAXS from lead aluminoborate glasses was used in classic experiments by Zarzycki and Naudin [23] to confirm Cahn's theory of spinodal decomposition [20] for compositions at the centre of the biphase region. A peak in the SAXS profile develops with time around wavevector, Q , of 0.04 \AA^{-1} (The scattering wavevector, Q , is given by $4\pi\sin\theta/\lambda$, where 2θ is the scattering angle and λ is the wavelength). As the phase separated microstructure ripens with annealing time this peak shifts to smaller Q values. The thermodynamic treatment predicts that X-rays will be diffracted from compositional fluctuations with a time dependent intensity, $I(Q,t)$, given by

$$I(Q,t) = I(Q,0) e^{2R(Q)t} \quad (8)$$

$$\text{where } R(Q)/Q^2 \propto Q^2.$$

$R(Q)$, the so-called ‘‘amplification factor’’, is sharply peaked at, $Q = 2\pi/\Lambda$, from which a ‘‘spinodal’’ wavelength, Λ , can be deduced. The initial stages of heat treatment of lead aluminoborate glasses [23] closely resembles these predictions and a value of 130 \AA is deduced for the spinodal wavelength, Λ . Similar behaviour has also been reported in the time-dependent annealing of glasses in the $(\text{Na}_2\text{O})_x(\text{SiO}_2)_{1-x}$ system [24].

The proportions by weight of the two phases in a phase-separated glass can be obtained using the ‘‘lever rule’’:

$$(x_2 - x)/(x - x_1) = M_1/M_2 \quad (9)$$

where x is the mean composition, x_1 and x_2 are the two phase separated compositions and M_1 and M_2 are the respective masses for a particular annealing temperature. From the known compositional dependent density, ρ_0 , of a silicate glass system, the mean square compositional density fluctuation, $\langle \Delta\rho^2 \rangle$, can be calculated for each value of x as well as the corresponding electron density contrast, $\langle \Delta\rho_e^2 \rangle$. The electron density contrast as a function of composition in the biphasic region for $(\text{Na}_2\text{O})_x(\text{SiO}_2)_{1-x}$ glasses calculated from Fig. 1 for the $T = 580^\circ\text{C}$ tie line is shown in Fig. 3. Compared to the immiscibility dome from which it is derived, $\langle \Delta\rho_e^2 \rangle$ versus x is symmetrical, with a maximum at $x \approx 0.1$. Close quantitative agreement has been found between curves such as this for different temperatures and the values deduced from absolute SAXS measurements for glasses annealed at these temperatures [16]. Fig. 3 also includes values of $\langle \Delta\rho_e^2 \rangle$ obtained from preliminary Landau-Placzek ratio measurements from $(\text{Na}_2\text{O})_x(\text{SiO}_2)_{1-x}$ glasses [8] using Eqs. 4 and 5. $\langle \Delta\rho_e^2 \rangle$ from R_{LP} measurements also peaks around $x = 0.1$. Earlier R_{LP} values for $(\text{K}_2\text{O})_x(\text{SiO}_2)_{1-x}$ glasses [9] indicate a maximum at $x < 0.1$, consistent with a narrower immiscibility zone in potassium silicate glasses.

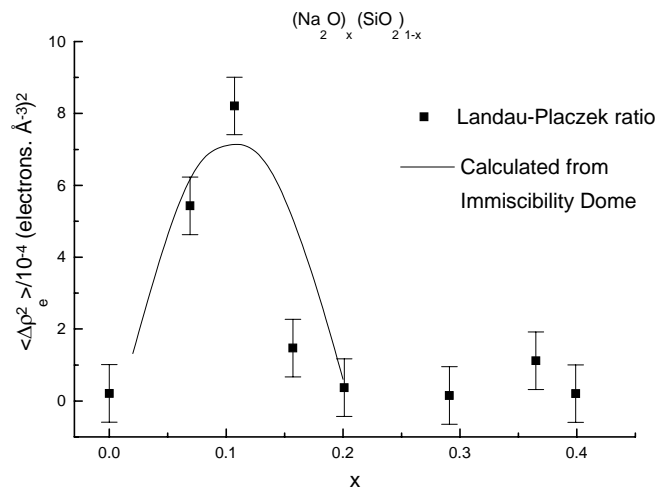


Fig. 3. Mean square density fluctuations obtained from Landau-Placzek Ratio measurements, R_{LP} , for $(\text{Na}_2\text{O})_x(\text{SiO}_2)_{1-x}$ glasses [8] using Eq. 4 (points). These are matched for a fluctuation volume, V , of $1.88 \times 10^4 \text{\AA}^3$ to the electron density contrast values, $\langle \Delta\rho_e^2 \rangle$, calculated from the phase separation density differences [15] given by the sub-liquidus coexistence curve

[18] plotted in Fig. 1.

In Fig. 3, the fluctuating volume, V , from Eq. (4), in this case for *compositional variations*, has been adjusted to match the $\langle \Delta\rho_e^2 \rangle$ values deduced from the sub-liquidus coexistence curve from Fig. 1. Best agreement is found for a volume of $1.88 \times 10^4 \text{\AA}^3$, equivalent to a cube of dimension 26.6\AA . This is much shorter than optical wavelengths and, indeed, unless sodium and potassium silicate glasses are heavily annealed, they are optically clear. $2\pi \cdot 26.6 \text{\AA}$ is similar in size to Λ , the “diffraction wavelength”, deduced from the development of SAXS intensity during the initial stages of spinodal decomposition [23,24]. 26.6\AA is also close to the value of 20\AA quoted earlier as the scale of *density fluctuations* in silica obtained from combining R_{LP} and I_0 measurements [14]. This raises the interesting question as to whether or not density fluctuations promote the compositional fluctuations that drive the development of phase separation. Finally it is also worth noting from Fig. 3 that for compositions *beyond* the immiscibility dome (i.e. $x > 0.2$), $\langle \Delta\rho_e^2 \rangle$ values deduced from R_{LP} observations using Eq. (4) and the same value of V return to the magnitude of $\langle \Delta\rho_e^2 \rangle$ for silica of $\sim 2 \times 10^{-5} [\text{electrons} \cdot \text{\AA}^{-3}]^2$. This demonstrates the monophasic character of silicate glasses outside the coexistence region. Here modified glasses share density fluctuations similar in magnitude to those in SiO_2 glass, and by the same token of similar length scale. Whether or not density fluctuations in single

phase sodium silicates are smaller in magnitude than in silica, as others have claimed [9] for potassium silicates, will require more precise Brillouin scattering experiments.

The dimensionality of the phase-separated microstructure can be probed through NMR spin relaxation by direct dipolar coupling to paramagnetic impurities introduced into the glass [25]. Originally applied to determine the fractal dimension of the mass distribution of ^{29}Si spins in silica gels [26], Sen and Stebbins [25] extended the technique to investigate both phase separated and monophasic Gd-doped Li and Na silicate glasses – Gd^{3+} being a suitable paramagnetic impurity. In the first place they observed differential spin relaxation for Q^3 and Q^4 species in $\text{Li}_2\text{Si}_4\text{O}_9$ glass which they found increased with annealing. By contrast no difference was found in the relaxation behaviour of Q^3 and Q^4 species in the monophasic $\text{Li}_2\text{Si}_2\text{O}_5$ and $\text{Na}_2\text{Si}_2\text{O}_5$ glasses. Q^n represents the SiO_4 tetrahedral configuration where Si is co-ordinated to n bridging oxygens (BO) and $4-n$ non-bridging oxygens (NBO). In Gd-doped glasses, Gd^{3+} will preferentially associate with Q^3 rather than Q^4 sites. From the coexistence curves for the Li silicate system [17], the tetrasilicate composition $\text{Li}_2\text{Si}_4\text{O}_9$ falls within the immiscibility dome and will be phase separated with lithia-rich and silica-rich regions. Since these glass phases are high in Q^3 and high in Q^4 , respectively, and because Gd^{3+} impurities group with the former, ^{29}Si relaxation rates for these two species are expected to be different in $\text{Li}_2\text{Si}_4\text{O}_9$ glass and the differences exaggerated by annealing, as Sen and Stebbins observed. On the other hand in $\text{Li}_2\text{Si}_2\text{O}_5$ and in $\text{Na}_2\text{Si}_2\text{O}_5$ glasses – compositions outside the coexistence regions - the spin relaxation behaviour for Q^3 and Q^4 configurations are found to be equivalent, confirming the monophasic character of these glasses and the intimate mixing of different configurations on the length scale of the experiment.

For the dipolar-paramagnetic coupling, for example between ^{29}Si spins and Gd^{3+} ions, the recovered magnetisation at a given time t , $M(t)$, is given by

$$M(t) \sim t^{D/6} \quad (10)$$

where D is the mass fractal dimension [26]. Interestingly Sen and Stebbins found that the recovery rate for ^{29}Si in $\text{Li}_2\text{Si}_4\text{O}_9$ glasses was significantly different from either $\text{Li}_2\text{Si}_2\text{O}_5$ or $\text{Na}_2\text{Si}_2\text{O}_5$ glasses. The two disilicate glasses both shared a more rapid ^{29}Si spin relaxation behaviour than the tetrasilicate glass. Using Eq. 10, they found $D = 2.62 \pm 0.22$ for the phase separated $\text{Li}_2\text{Si}_4\text{O}_9$ glasses but $D = 3.06 \pm 0.18$ for the monophasic $\text{Li}_2\text{Si}_2\text{O}_5$ and $\text{Na}_2\text{Si}_2\text{O}_5$ glasses. The power law regimes observed for $\text{Li}_2\text{Si}_4\text{O}_9$ and for $\text{Li}_2\text{Si}_2\text{O}_5$ and $\text{Na}_2\text{Si}_2\text{O}_5$ glasses [25] are reproduced in Fig. 4 and Fig. 5, respectively. Note that Q^3 and Q^4 species in each glass share the same power law dependence for ^{29}Si magnetisation recovery, including the $\text{Li}_2\text{Si}_4\text{O}_9$ glass where the strength of the Q^3 signal (open symbols) is greater than the Q^4 signal (Fig. 4).

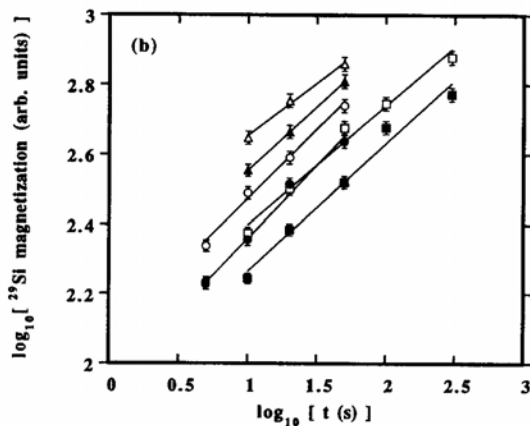


Fig. 4. Power law regimes in ^{29}Si magnetisation recovery for phase separated $\text{Li}_2\text{Si}_4\text{O}_9$ glasses with different Gd_2O_3 doping levels [25]. The open symbols refer to ^3Q species and the closed symbols to ^4Q species. Although the magnitudes are different, the slopes, $D/6$ in Eq. 6, are the

same within experimental error. See text for details.

For this glass, though, the value of $D = 2.62$ is close to the mass fractal dimension 2.6 for an infinite percolation cluster [27]. This is entirely consistent with the interconnectivity observed in nucleated phase separated Li silicates *off-centre* from the immiscibility dome [28]. Fig. 2 illustrates the case for fully developed phase separation in an annealed Na silicate glass [16]. It is worth mentioning that spinodal decomposition, which occurs on-centre in the coexistence region, is not expected to exhibit a fractal geometry [29]. By comparison from Fig. 5, Euclidean geometry is recorded for Q^n species ($D = 3.06$) in the disilicate compositions $\text{Li}_2\text{Si}_2\text{O}_5$ and $\text{Na}_2\text{Si}_2\text{O}_5$. This is expected for the overall silicate network of these single-phase glasses on the length scale of the technique. NMR spin relaxation measurements probe a few 10's Å to a few 100's Å [25]. They therefore overlap with the length scale of Brillouin Scattering and, from the results shown in Fig. 3, should extend down to Q ($\sim V^{1/3}$) = 0.04 Å⁻¹ in the SAXS regime.

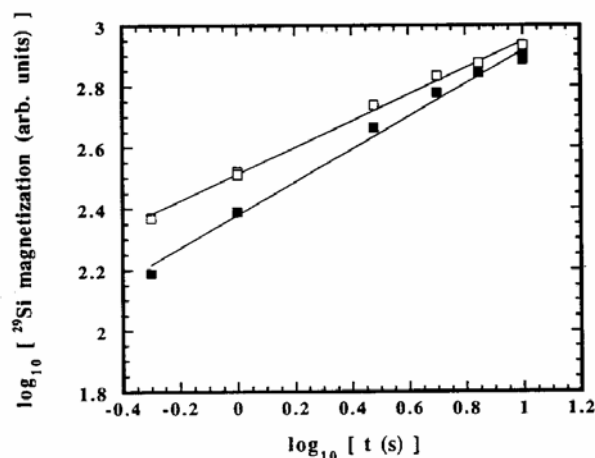


Fig. 5. Power law regimes in ^{29}Si magnetisation recovery for monophasic silicate $\text{Li}_2\text{Si}_2\text{O}_5$ and $\text{Na}_2\text{Si}_2\text{O}_5$ glasses [25]. Because there is no differential spin relaxation amongst ^{29}Q species,

the total ^{29}Si signal has been used. See text for details.

It is important to stress again that, in the absence of excessive heat treatment, Li and Na silicate glasses are optically clear. Accordingly, phase separation is not just a feature of opalescent glasses (Fig. 2), although the geometry of the interlacing phases may be scale invariant. On the shortest length scale so far discussed of a few 10's Å, the geometric magnitude of phase separation in silicate glasses is close to that of density fluctuations. However, modified glasses also exhibit microheterogeneity on length scales far finer than this and close to atomic dimensions in size.

4. Local order, long range order and phase separation

Quite apart from density fluctuations and phase separation, microstructure deriving from the microsegregation of network modifiers from network formers was predicted in silicate glasses from the very first Na, K and Ca XAFS experiments [30,31]. These confirmed that well-defined short-range order was present around modifying cations. Na XAFS Fourier transforms for two oxides glasses - a silicate and an aluminosilicate - are compared in Fig. 6(a) [32,33], where the principle nearest neighbour oxygen shell around 2.4 Å is clearly in evidence, including the presence of Na-Na correlations approximately 3.5 Å. Indeed in the crystalline state [34] the distance between alkalis in adjacent silicate units is very similar in size to this value. The different local order around sodium in the two glasses, resulting from the different glass former compositions, is illustrated in Fig. 6(b) by the differences in the oxygen co-ordination number, N , and in the variance of the oxygen distances, $2\sigma^2$.

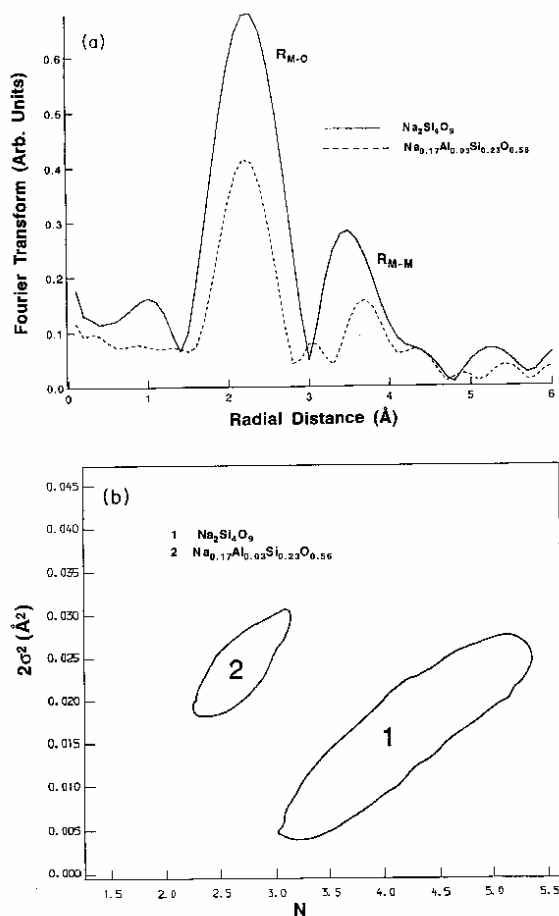


Fig. 6. Local atomic arrangements around Na from Na XAFS in two different silicate glasses: $\text{Na}_2\text{Si}_4\text{O}_9$ (solid line) and $\text{Na}_{0.17}\text{Al}_{0.03}\text{Si}_{0.23}\text{O}_{0.56}$ (dashed line) [32]. (a) Partial rdf's obtained from Fourier Transforming Na XAFS, differentiating nearest neighbour oxygens, R_{M-O} , from nearest neighbour sodiums, R_{Na-Na} . (b) Results of least square fitting of experiment to theory shown in the form of Debye-Waller ($2\sigma^2$) versus Coordination Number (N_{Na-O}) correlation maps. 95% significance contours clearly distinguish the well - defined local order in these two

different glasses.

Taken in conjunction with the strong tetrahedral configuration of silicons established in the earliest X-ray measurements [2], observations of local order around modifying cations, such as Na, led to the modified random network model (MRN) for oxide glasses [32] illustrated in Fig. 7(a) [33]. Long range order in the MRN model is characterised by interpenetrating modifier and network components and the resulting microstructure should lead to a fractal geometry on the nanoscale similar to that observed in incipient phase separation [25] but on a smaller length scale. In the case of alkali microsegregation the percolation threshold [27] will be reached once the modifier component, x , has reached 16% [32]. Below 16%, individual islands of alkali clusters are expected within the partially depolymerised silicate network. Such long range order is also a natural outcome of molecular dynamics (MD) simulations of silicate glass structure [35, 36, 37]. Fig. 7(c) illustrates this for sections taken through MD simulations for a sequence of $(\text{Na}_2\text{O})_x(\text{SiO}_2)_{1-x}$ glasses where the alkali content is increasing (left to right) from $x = 0.05$ to $x = 0.3$ [36]. The development of microsegregation is very obvious. The middle frame in Fig. 7(c) corresponds to $x = 0.2$, just above the percolation threshold.

Fig. 7(b) illustrates the principles of the MRN model extended to an aluminosilicate glass structure. Here, aluminiums are fully charge-compensated by alkalis and there are no NBO's. This "compensated" continuous random network, or CCRN, is fully connected like silica [33]. However, since odd member rings are not prevented, Lowenstein's Rule of chemical order that describes

crystalline aluminosilicates will not necessarily apply to glasses of equivalent composition. Some clustering of aluminiums and therefore of charge compensating modifying cations is expected, as Fig. 7(b) illustrates and Fig. 6 supports through the modelling of Na-Na correlations [33].

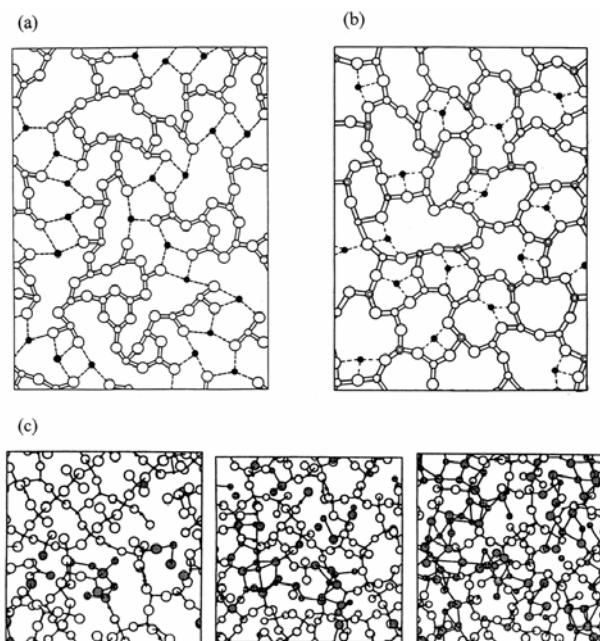


Fig. 7. Random Network models for silicate glasses. (a) Modified Random Network model (MRN) which includes BO's and NBO's charge compensated by modifying cations [32]. (b) Compensated CRN (CCRN) for aluminosilicate glasses which excludes NBO's but where aluminiums are charge compensated by modifying cations [33]. Clustering of modifying cations is evident in both models. For larger MD models quasiperiodic structure is observed (see Fig. 12). (c) MD simulations of $(\text{Na}_2\text{O})_x(\text{SiO}_2)_{1-x}$ glasses [36]. In these sections, Na's and NBO's are shown shaded. With the modifier content increasing from left to right, $x = 0.05$, 0.2 and 0.3 and microsegregation is evident, even in the most dilute case. Channels become

established above the percolation threshold $x = 0.16$ [27].

Additional evidence for alkali microsegregation in silicate glasses has been obtained from solid state ^{17}O NMR which can be used to distinguish bridging from terminal oxygens in potassium silicate glasses i.e. BO's from NBO's [38]. Also the preferential co-ordination of potassium to NBO's has been detected. As modifying cations are also highly co-ordinated to NBO's [31,32], a picture of the close-packing of NBO's and modifying cations emerges which geometrically is bound to result in some degree of microsegregation of glass modifier from glass former. Furthermore new developments in double resonance ^{29}Si have revealed that correlations exist between different Q^n species [39, 40], notably Q^3 species. As Q^3 's share NBO's with modifying cations, this again points to clustering of the modifying component. The fact that such long range order is not seen in NMR spin relaxation (Fig. 5), where the bulk fractal dimension, $D \sim 3$, is because alkali microsegregation occurs on a length scale much smaller than the minimum length scale for magnetisation recovery of several 10^3 \AA [25]. Finally, recent analysis of the neutron scattering pattern from $\text{K}_2\text{Si}_4\text{O}_9$ glass using Reverse Monte Carlo techniques has also resulted in a model structure in which K atoms cluster, despite a starting structure in which the alkalis were uniformly distributed [41].

Returning to Fig. 7 it is clear from the long range order present in MRN and CCRN models that compositional variations exist on the subnanometre scale. In particular, local order does not extend homogeneously into the regime of density fluctuations and phase separation. Indeed, from the MD calculations of binary $(\text{Na}_2\text{O})_x(\text{SiO}_2)_{1-x}$ glasses [e.g. 36], when $x < \sim 0.2$ and alkali channels are incomplete, the structure is necessarily microphase separated, with sodium-rich and silica-rich regions. There is every reason to suppose that this long range order is also present below the liquidus.

We speculate, therefore, that these are the fluctuations in composition, x , from which incipient phase separation will nucleate, rather the density fluctuations

$$k_B T_f (K_T - K_S + K_S^r)$$

frozen in at the glass transition (Eq. 2). At the same time we anticipate that the density fluctuations will limit the extent to which the long-range order that stems from local order persists.

5. Microsegregation and quasiperiodicity

Because density fluctuations and, for glasses with compositions in the coexistence regime, phase separation are ubiquitous throughout the structure of a glass, we should only expect to find evidence for the long range order stemming from modifier microsegregation on length scales shorter than $V^{1/3}$ or $\Lambda/2\pi$. Local atomic order is usually described in terms of the total radial distribution function, $T(r)$, and this is plotted for a typical oxide glass, $\text{Na}_2\text{Si}_2\text{O}_5$ [42] in Fig. 8(a). The contribution from Na-O correlations at 2.4 Å, clearly seen in Na XAFS (Fig. 6), can be identified by the shoulder between the strong Si-O (1.6 Å) and O-O (2.6 Å) peaks coming from corner-shared SiO_4 tetrahedral units. The experimental neutron scattering pattern, $Q_i(Q)$, from which $T(r)$ is obtained is also plotted in Fig. 8(b). Experimental values for both $T(r)$ and $Q_i(Q)$ are directly compared with an MD structure simulated for $\text{Na}_2\text{Si}_2\text{O}_5$ glass [35] in Fig. 8, which demonstrates the particularly good agreement that can be obtained in both wavevector and real space by computer modelling [43]. From Fig. 8 wide angle diffraction quite clearly starts above 1 \AA^{-1} . Accordingly, evidence for modifier microsegregation in silicate glasses should be found in the wave vector window between approximately 0.05 \AA^{-1} ($V^{1/3}$) and 1 \AA^{-1} .

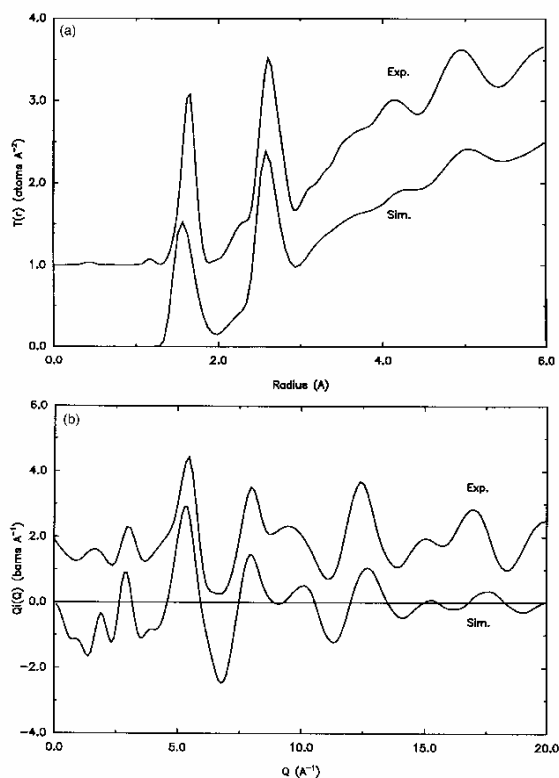


Fig. 8. The total rdf ($T(r)$) (a) and the weighted structure factor, $Q_i(Q)$, (b) for $\text{Na}_2\text{Si}_2\text{O}_5$ glass obtained from neutron scattering (Exp) [42] compared to the predictions from an MD model (Sim) at 1000 K [43]. Note the FSDP at 1.8 \AA^{-1} . This can be related to the Na-Na correlations of spacing around 3.6 \AA (see Fig. 6) and the quasiperiodicity evident in the model projection (Fig. 2).

Initial SAXS measurements in this range for alkali silicate and borate glasses have revealed marked differences between modified glasses and glass formers like silica [44]. As alkali was added to the glass composition, the scattering was observed to increase substantially between 0.03 \AA^{-1} and 0.1 \AA^{-1} . It also became more pronounced the heavier the alkali-type. We have recently made a more detailed SAXS study of $(\text{Na}_2\text{O})_x(\text{Si}_2\text{O}_5)_{1-x}$ glasses [45], using the same samples employed for Brillouin scattering [8] discussed earlier in connection with Fig. 3. Preliminary SAXS results for silica and for $\text{Na}_2\text{Si}_3\text{O}_7$ glass are plotted in Fig. 9. These profiles are also merged with the initial First Sharp Diffraction Peaks (FSDP) obtained from X-ray scattering for the same glasses. Plotted as $\ln I$ versus $\ln Q$, Fig. 9 clearly identifies the wavevector window of 0.05 \AA^{-1} to 1 \AA^{-1} and the way that this is filled in when Na_2O is added to silica. It also reveals a common $I \propto Q^{-4}$ regime below $\sim 0.04 \text{ \AA}^{-1}$ for both glasses. There are also differences in the height and position of the FSDP with composition, which we shall return to later.

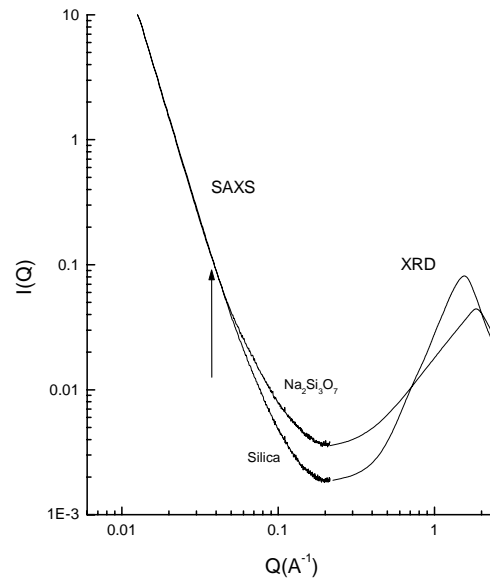


Fig. 9. Scattering from silicate glasses in the window between SAXS and the start of the structure factor $S(q)$, $\log I$ versus $\log Q$ from 10^{-2} \AA^{-1} to 2 \AA^{-1} . Recent SAXS measurements [45] have been merged with X-ray Diffraction (XRD) results [46] for SiO_2 and $\text{Na}_2\text{Si}_3\text{O}_7$ glass.

The morphology of complex inorganic and organic composites, like silica gels and porous glasses, have been traced over many decades of length scale by combinations of light scattering, SAXS and XRD [29, 47]. When microstructure is nucleated from similar sized particles two scattering regimes can usually be delineated. In descending length scale (increasing Q) this sequence starts with Guinier's law

$$I \propto \exp(-Q^2 R_g^2/3), \quad (11)$$

which describes the scattering by the monodispersed particle agglomerates, and ends with Porod's law

$$I \propto Q^P \quad (12)$$

which relates to the scattering from internal surfaces within the particles [12], where

$$P = -2D + D_s \quad (13)$$

For mass fractals, surface area scales with mass, so $D = D_s$ in which case $P = -D$, the bulk fractal dimension. Because surface fractals are uniformly dense $D = 3$ and $P = -6 + D_s$, where D_s is

the surface fractal dimension. For smooth interfaces $D_S = 2$ and $P = -4$ as we find for scattering from silicate glasses in Fig. 9. For rough interfaces, though, $D_S < 2$ and $P < -4$ and for diffuse interfaces $D_S > 2$ and $P > -4$ [29]. The different scattering regimes are schematically contrasted with diffraction in Fig. 10 whilst in Fig. 11 the X-ray scattering simulated from the MD model of $\text{Na}_2\text{Si}_2\text{O}_5$ glass [35,43] introduced in Fig. 8 is plotted. Like Fig. 9, Fig. 11 incorporates both the SAXS and the wide angle XRD regime [44].

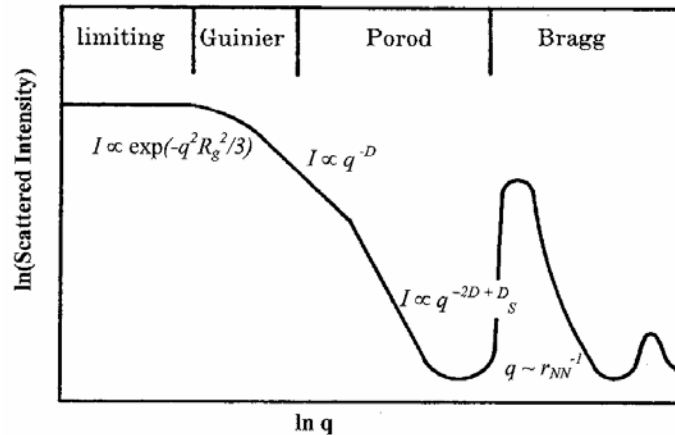


Fig. 10. Schematic showing the different regimes for scattering from a nucleated microstructure compared to Bragg diffraction [from 29]. Plotted as $\ln I$ versus $\ln Q$, on the longest length scale scattering is from the largest particles (Guinier). The Porod regime beyond this comprises scattering from mass distribution within the particles ($I \propto Q^{-D}$) and ultimately scattering of domain interfaces ($I \propto Q^{-6 + D_s}$), where D is the mass fractal dimension and D_s the

surface fractal dimension. Finally Bragg diffraction follows at the largest Q .

In present context, the Q^{-4} regime in Fig. 9 found experimentally for both silica and $\text{Na}_2\text{Si}_3\text{O}_7$ glass can be associated with scattering from smooth interfaces of nm size. Since both glasses are monophasic on this scale, we can ascribe these interfaces to those generated by density fluctuations. As we have seen the magnitude of density fluctuations for both glasses determined from Brillouin scattering (Fig. 3) are the same within experimental error. Interestingly, $I \propto Q^{-4}$ scattering can also be seen in Fig. 11 for the scattering calculated from an 8640 atom model for $\text{Na}_2\text{Si}_2\text{O}_5$ glass. This was assembled from 8 units of the 1080 atom MD model [43,44]. Although this structure was subsequently relaxed, scattering from the original 24 Å box size clearly remains in the strong interference fringes. Since the box size is close to the experimental $V^{-1/3}$ values obtained from R_{LP} and SAXS, the average Q^{-4} trend in Fig. 11 can be considered crudely to model density fluctuations in the monophasic glass. The fact that the *magnitude* of the calculated Porod scattering is greater for the model (Fig. 11) compared to experiment (Fig. 9) reflects the sharper interface in the model due to the box size compared to the interfaces between density fluctuations in real glasses.

Returning to Fig. 9, the $I \propto Q^{-4}$ behaviour exhibited by both silica and $\text{Na}_2\text{Si}_3\text{O}_7$ glass continues out to $Q \sim 0.04 \text{ \AA}^{-1}$, at which point scattering from the two glasses bifurcate. The power law weakens more for $\text{Na}_2\text{Si}_3\text{O}_7$ glass than for silica, the initial $\ln - \ln$ slopes for the two glasses being -3 and -2.4 respectively. This is reminiscent of scattering from bulk mass fractals and is indicative of new microstructure for both glasses but on a length scale less than 20 Å.

Scattering from nested multiple scale microstructures [29, 46], generally exhibit overlapping Porod and sometimes Guinier regimes. Finer structure emerges as the wavevector Q increases, the reciprocal of the wavevector at the overlap providing an indication of the size of coarser domain. In Fig. 9, the weakening of the power law for the two glasses and the splitting of the silica profile from that of $\text{Na}_2\text{Si}_3\text{O}_7$ glass occurs when the wavelength of the X-rays is smaller than the size of the density

fluctuations, which have already been quantified in silicate glasses as being around 20 Å [14]. Similar behaviour is modelled in the SAXS profile calculated for the simulated glass in Fig. 11. The arrow in Fig. 9 marks $q = V^{-1/3} = 1/26.7 \text{ \AA}^{-1}$ obtained from fitting R_{LP} for phase separated $\text{Na}_2\text{O} - \text{SiO}_2$ glasses in Fig. 3, adding further evidence to a common scale for the density fluctuations and phase separation in silicate glasses. It is beyond the point marked by the arrow in Fig. 9 that scattering from smaller-scale microstructure emerges.

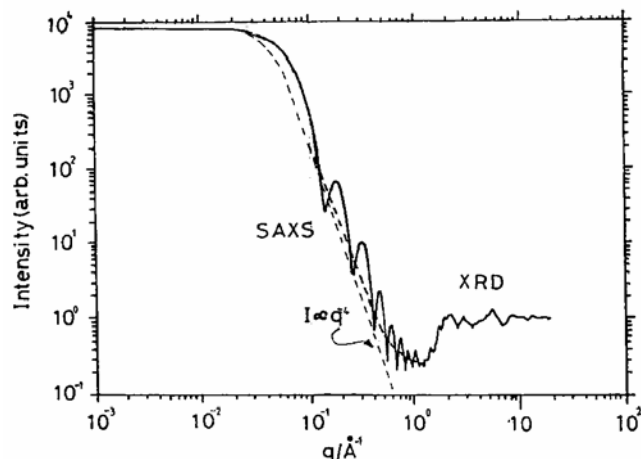


Fig. 11. Total X-ray Scattering predicted for a 8640 atom model of $\text{Na}_2\text{Si}_2\text{O}_5$ glass assembled from the MD structure whose rdf and structure factor are shown in Fig. 8(a) with the real space structure in Fig. 12 [44]. The interference fringes in the SAXS regime result from scattering from the original 24 Å box size of the 1080 atom model [35] but additional scattering can be seen $q > 0.1 \text{ \AA}^{-1}$, leading eventually to interatomic diffraction in the form of the model

structure factor.

The MRN model for modified silicate glasses predicts microsegregation, comprising interconnecting channels of alkali surrounded by silica network as depicted in Fig. 7(a). Fig. 12 shows a section through the MD model of Na_2SiO_5 glass [36,43] described earlier (Fig. 7). This clearly reveals microsegregation of glass modifier from glass former, as earlier MD studies have reported [36]. Given the box size of 24 Å, the quasiperiodic spacing can be judged to be between 3 and 4 Å. This close to the mean Na-Na distance [35] in the MD model, which is also found experimentally from XAFS (see Fig. 6(a)) [30-33]. The geometry of this long-range order is expected to be of low dimension, mirroring the chain and layer structures of crystalline silicates [34]. Accordingly, the power law measured for $\text{Na}_2\text{Si}_3\text{O}_7$ glass ($I \propto Q^{-2.4}$) beyond $Q \sim 0.04 \text{ \AA}^{-1}$ in Fig. 9, which points to a mass fractal dimension of 2.4, is strong evidence for alkali microsegregation in modified glasses. Indeed we find that this trend continues for other $(\text{Na}_2\text{O})_x (\text{Si}_2\text{O}_5)_{1-x}$ glasses as the Na_2O content, x , increases further [45], the SAXS for all the silicate glasses branching at the same wavevector ($Q = \sim 0.04 \text{ \AA}^{-1}$) – including, incidentally, glasses in the coexistence region.

Extending a similar interpretation to the SAXS pattern for silica in Fig. 9, the observed power law of $I \propto Q^{-3}$ indicates a mass fractal dimension $D = 3$. The presence of another level of microstructure in silica, on a finer scale than density fluctuations, is at first unexpected. All the modelling studies for this classic glass [48, 49, 50, 51, 52] point to an isotropic homogeneous structure on the scale of 10's Å. However, heterogeneity in the form of quasiperiodicity with a repeat distance $\sim 3.4 \text{ \AA}$ has recently been analysed from the large scale modelling of a-Si [53]. Indeed, very fine density fluctuations are revealed in the model rdf beyond around 10 Å. This quasiperiodicity is reproduced in Fig. 13 for a model section with a box size of 66.5 Å. Scaling this tetrahedral network to mimic silica by replacing Si-Si (2.38 Å) by Si-O-Si (3.1 Å) enlarges the box size in Fig. 13 from 66.5 Å to 90 Å and raises the repeat distance from $\sim 3.4 \text{ \AA}$ to $\sim 4.1 \text{ \AA}$. Whilst there is some indication from the experimental rdf of silica for residual periodicity at large distances in the region of 4 Å [53],

the strongest evidence for quasiperiodicity in silica and indeed in other silicate glasses comes from the location and width of the FSDP.

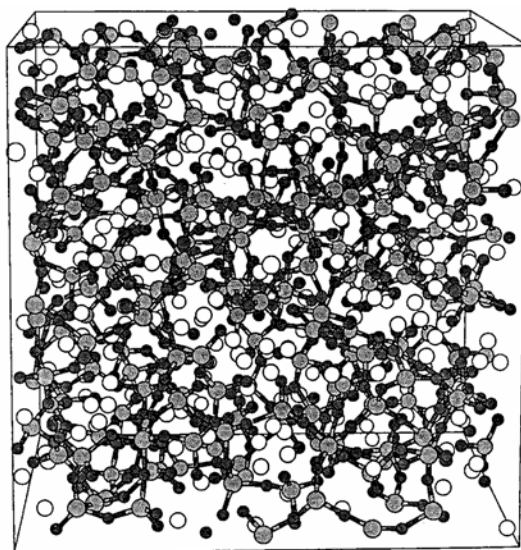


Fig. 12. Quasiperiodicity predicted from MD modelling studies of $\text{Na}_2\text{Si}_2\text{O}_5$ glass [35,43,44]. The network is shown shaded, with sodiums identified by open circles. The box size is 24 \AA and the quasiperiodic spacing is approximately 3 to 4 \AA . This matches the Na-Na correlations

in the model and what is observed from Na XAFS [33] in Fig. 6(a).

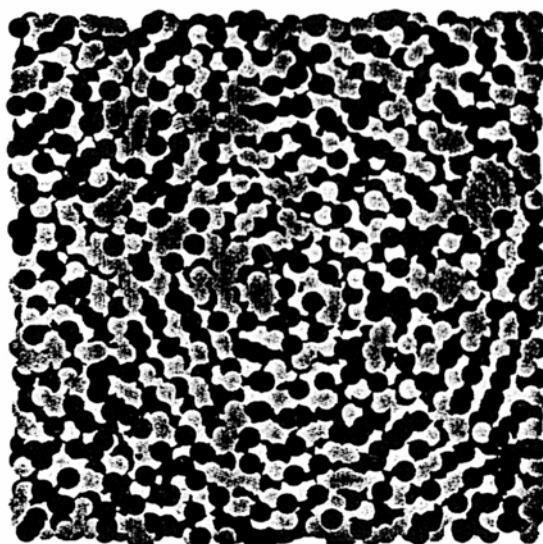


Fig. 13. Quasiperiodicity revealed from modelling studies of a-Si [53]. The contrast is between neighbours connected by odd numbered chains (grey) and even numbered chains (black). These mirror the contrast between voids and atoms in the tetrahedral structure. Scaling up to replicate silica by replacing Si-Si by Si-O-Si results in a quasiperiodic spacing of $\sim 4.1 \text{ \AA}$

and a box size of $\sim 90 \text{ \AA}$.

6. The first sharp diffraction peak (FSDP)

There has been much discussion as to the origin of the FSDP in network glasses [54], not least in its definition. Assuming that this is indeed a Bragg peak, the FSDP at Q_{FSDP} will contribute to interatomic correlations R_{FSDP} given by

$$R_{FSDP} \approx 2\pi/Q_{FSDP} \quad (14)$$

Accordingly, with Q_{FSDP} falling at values between 1 \AA^{-1} to 2 \AA^{-1} , this diffraction relates to interatomic correlations R_{FSDP} in the range 3 \AA to 4 \AA . In the total rdf, $T(r)$, like the one plotted in Fig. 8(a), R_{FSDP} falls in the vicinity of fourth nearest neighbours where changes between different glasses are difficult to interpret without 3 dimensional models. This originally added confusion when the origins of the FSDP were first considered [54 and references therein]. Given that the FSDP is a Bragg peak, then the correlation length, L_{FSDP} , which measures the range over which the periodicity is maintained in the glass, is related to the width of the peak (FWHM) [55], ΔQ_{FSDP} , by

$$L_{FSDP} \approx 2\pi/\Delta Q_{FSDP} \quad (15)$$

The FSDP for silica and for $\text{Na}_2\text{Si}_3\text{O}_7$ glass can be clearly seen in Fig. 9 at 1.5 \AA^{-1} and 1.8 \AA^{-1} respectively, as well as in the neutron scattering pattern of $\text{Na}_2\text{Si}_2\text{O}_5$ glass (Fig. 8(b)). By contrast the structure factor “proper” for silicate glasses commences at $Q > \sim 2.5 \text{ \AA}^{-1}$ ($2\pi/r_{\text{O-O}}$ neutrons) and $> \sim 4 \text{ \AA}^{-1}$ ($2\pi/r_{\text{Si-O}}$ X-rays). It is noteworthy from Fig. 9 that the magnitude of the FSDP for X-rays is reduced for $\text{Na}_2\text{Si}_3\text{O}_7$ glass compared to silica, which bears out the results of earlier neutron scattering studies of silica and Na and Li disilicate glasses [56] where similar behaviour was reported. In more recent neutron scattering measurements of $(\text{Na}_2\text{O})_x(\text{SiO}_2)_{1-x}$ glasses for $0 > x > 0.4$ [42], the FSDP can be seen to reduce in magnitude and also to shift to larger Q with increased Na_2O content. These changes in the position and shape of the FSDP for silica compared to silicate glasses have so far not been discussed in the literature. Fig. 14 illustrates equivalent behaviour in the FSDP for $(\text{K}_2\text{O})_x(\text{SiO}_2)_{1-x}$ glasses [57], where the peak position clearly moves to larger Q with increasing x , viz. from 1.5 \AA^{-1} for silica to 2.0 \AA^{-1} for $\text{K}_2\text{Si}_3\text{O}_7$ glass.

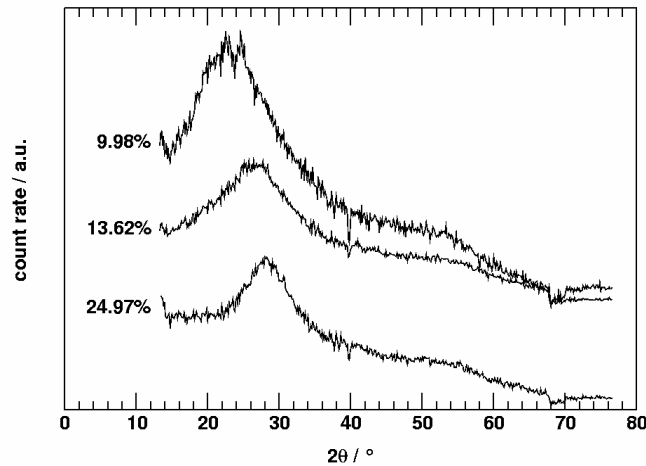


Fig. 14. First Sharp X-ray Diffraction Peaks measured in $(\text{K}_2\text{O})_x(\text{SiO}_2)_{1-x}$ glasses [57]. Note the shift of the peak to larger Q with increasing alkali content.

The FSDP can be computer modelled quantitatively, provided box sizes are sufficiently greater than L_{FSDP} . A distorted version of the FSDP at $\sim 2 \text{ \AA}^{-1}$ can be seen in the MD simulations of $\text{Na}_2\text{Si}_2\text{O}_5$ glass in Fig. 8(b) [35] and in Fig. 11 [44]. In modelling silica, Nakano and coworkers [52] have stressed how the size of the FSDP increases with the model size, correlations in the 4 \AA to 11 \AA range playing a vital role. These interatomic distances embrace the 4-bond neighbours – Si-O(2) and O-Si(2) – and are prominent in 5- and 6-fold rings [50]. More generally the FSDP has been

interpreted qualitatively on the molecular structure inherent in network glasses and melts, medium range order arising from cluster-cluster correlations or from ordering of the voids generated between them [54, 58]. For silicate glasses, on the other hand, the modifier component depolymerises the silica network which in principle will affect the ring statistics. In addition, alkali oxide modifiers bring charged NBO anions and alkali cations into the structure. In completely polar systems ionic interactions can give rise to Coulomb ordering [59,60] and these affects may also be influential in determining the intermediate range order in modified silicates. At the same time the inclusion of Na₂O or K₂O will remove some of the voids that are believed to characterise medium range order in AX₂ – type systems [58].

Table 1. Experimental positions (Q_{FSDP}) and widths (ΔQ_{FSDP}) for First Sharp Diffraction Peaks (FSDP) for silica compared to Na and K silicate glasses. Quasiperiodic spacings (R_{FSDP}) and

Correlation Lengths (L_{FSDP}) are shown alongside.

| | $Q_{FSDP}/\text{\AA}^{-1}$ | $\Delta Q_{FSDP}/\text{\AA}^{-1}$ | $R_{FSDP}/\text{\AA}$ | $L_{FSDP}/\text{\AA}$ | References |
|--|----------------------------|-----------------------------------|-----------------------|-----------------------|------------|
| SiO ₂ | 1.5 | 0.4 | 4.1 | 15.7 | [61] |
| Na ₂ Si ₃ O ₇ | 1.8 | 1.2 | 3.5 | 5.2 | [45] |
| Na ₂ Si ₂ O ₅ | 1.7 | 0.6 | 3.7 | 10.5 | [42] |
| K ₂ Si ₁₉ O ₃₉ | 1.5 | 0.5 | 4.2 | 13.8 | [57] |
| K ₂ Si _{6.4} O _{13.8} | 1.9 | 0.7 | 3.4 | 8.5 | [57] |
| K ₂ Si ₃ O ₇ | 2.0 | 0.5 | 3.2 | 12.7 | [57] |

The simplest interpretation of the FSDP, certainly in the silicate glasses we are discussing, is that this is the Bragg peak associated with the quasiperiodicity that constitutes the long range order identified from SAXS for $Q > \sim 0.04 \text{\AA}^{-1}$ in Fig. 9. Such microstructure exists on a length scale much shorter than the size of 20 Å characterised for density fluctuations and phase separation from R_{LP} . Whilst much experimental information about FSDP's is available for classic single and two component glasses [54], like silica for example [61], little is catalogued for more complex systems, like the modified silicate glasses under review. We have therefore drawn together in Table 1, values for the FSDP positions and widths, Q_{FSDP} and ΔQ_{FSDP} , for the Na and K silicates discussed in this paper. Using Eq. 14 and Eq. 15, values for the corresponding quasiperiodic spacings (R_{FSDP}) and correlation lengths (L_{FSDP}) are presented. Three simple points can be concluded:

1. R_{FSDP} values for silica and for sodium disilicate indeed fall close to the respective quasiperiodic spacings of 4.1 Å and 3.5 Å deduced from models [35,53] and from experiment [32]. Hence we feel confident in making the connection between changes in the FSDP and in the SAXS that is intuitively evident in Fig. 9.
2. The correlation length L_{FSDP} for silica of 16 Å approaches the 20 Å size that we have determined for density fluctuations. This points to the fact that *in the absence* of thermodynamic fluctuations in the melt quasiperiodicity in silica might extend still further, as indeed modelling studies suggest [53]. Note that the most dilute potassium silicate, $x = 0.05$, also has similar L_{FSDP} values.
3. For intermediate concentrations of sodium and potassium in silicate glasses the correlation lengths, L_{FSDP} , are very much shorter than for silica: typically 5 to 10 Å. If the long range order in these structures adheres to the MRN concept of interpenetrating modifier and network sublattices, then we can expect the existence of two quasiperiodic spacings which, with close mixing, will mutually interact to reduce the overall correlation length.

7. Conclusions

Density fluctuations in monophasic silicate glasses occur on the same length scale of around 20 Å as incipient phase separation for coexistent compositions. On a finer scale quasiperiodic structure exists which is derived from the local atomic structure. The coherence length of this miniature microstructure is restricted in single phase glasses by density fluctuations whilst in binary

glasses it is substantially reduced because of the mixing of two quasiperiodic structures with different spacings – one related to microdensity fluctuations in the silicate network and the other to alkali microsegregation. It would appear that phase separation is nucleated from such compositional and structural fluctuations.

Acknowledgements

The support of CNRS and CLRC is gratefully acknowledged for providing experimental light scattering and synchrotron radiation facilities. Florian Menau and Aled Jones are thanked for assistance in preparing some of the details of this paper.

References

- [1] W. H. Zachariasen, *J. Am. Chem. Soc.* **54**, 3841 (1932).
- [2] B. E. Warren, J. Biscoe, *J. Am. Ceram. Soc.* **21**, 49 (1938).
- [3] L. D. Landau, E. M. Lifshitz, *Statistical Physics*, Addison-Wesley, Reading MA (1969), Chapter 12 (1969).
- [4] N. L. Laberge, V. V. Vasilescu, C. J. Montrose, P. B. Macedo, *J. Am. Ceram. Soc.* **56**, 506 (1973).
- [5] I. L. Fabelinskii, *Molecular Scattering of Light*, Plenum Press, NY (1968).
- [6] J. Schroeder, in *Treatise on Materials Science and Technology*, ed. M. Tomozawa and R. H. Doremus, Academic Press, NY (1977), Vol 12.
- [7] J. A. Buccaro, H. D. Dardy, *J. Appl. Phys.* **45**, 2121 (1974).
- [8] Y. Vaills, *L'Habilitation à Diriger des Recherches à Université d'Orleans*, 76 (1999).
- [9] J. Schroeder, R. Mohr, P. B. Macedo, C. J. Montrose, *J. Am. Ceram. Soc.* **56**, 510 (1973).
- [10] D. L. Weinberg, *J. Appl. Phys.* **33**, 1012 (1962).
- [11] A. Pierre, D. R. Uhlmann, *J. Appl. Cryst.* **5**, 216 (1972).
- [12] A. Guinier, G. Fournet, *Small Angle Scattering of X-rays*, Wiley, NY (1955).
- [13] E. A. Porai-Koshits in *Borate Glasses*, ed. L. D. Pye, V. D. Frechette, N. J. Kreidl, Plenum, NY (1970) pp. 183.
- [14] J. Zarzycki in *Glasses and the vitreous state*, Cambridge University Press, Cambridge 148 (1991).
- [15] V. L. Averjanov, N. S. Andreev, E. A. Porai-Koshits in *Physics of Non-Crystalline Solids* Ed. J. A. Prins, North Holland, Amsterdam p. 580, 1965.
- [16] E. A. Porai-Koshits, V. I. Averjanov, *J. Non-Cryst. Solids* **1**, 29 (1968).
- [17] R. J. Charles, *J. Am. Ceram. Soc.*, **49**, 55 (1966).
- [18] W. Haller, D. H. Blackburn, J. H. Simmons, *J. Am. Ceram. Soc.* **57**, 120 (1974).
- [19] E. Z. Scheil, *Z. Metallik*, **43**, 40 (1950).
- [20] J. W. Cahn, *J. Chem. Phys.* **42**, 93 (1965); J. W. Cahn, R. J. Charles, *Phys. Chem. Glasses* **6**, 181 (1965).
- [21] J. W. Cahn, *Chem. Phys.* **42**, 93 (1965).
- [22] W. Haller, *J. Chem. Phys.* **42**, 686 (1965).
- [23] J. Zarzycki, F. Naudin, *J. Non-Cryst. Solids* **1**, 215 (1969).
- [24] M. Tomozawa, R. K. MacCrone, H. Herman, *Phys. Chem. Glasses* **11**, 136 (1970).
- [25] S. Sen, F. J. Stebbins, *Phys. Rev.* **50**, 822 (1994).
- [26] F. Devreux, J. P. Boilot, F. Chaput, B. Sapoval, *Phys. Rev. Lett.* **65**, 614 (1990).
- [27] R. D. Zallen, *The Physics of Amorphous Solids*, Wiley, New York (1983).
- [28] R. J. Charles, *J. Am. Ceram. Soc.* **46**, 235 (1963).
- [29] D. W. Schaefer, B. C. Bunker, J. P. Wilcoxon, *Proc. Roy. Soc. Lond.* **A 423**, 35 (1989).
- [30] G. N. Greaves, A. Fontaine, P. Lagarde, D. Raoux, S. J. Gurman, *Nature* **293**, 611 (1981).
- [31] G. N. Greaves in *Glass Science and Technology* Ed. D. Uhlmann, N. J. Kreidl, Academic Press, New York, p.1, 1990.
- [32] G. N. Greaves, *J. Non-Cryst. Solids* **71**, 203 (1985).
- [33] G. N. Greaves, K. L. Ngai, *Phys. Rev.* **B 52**, 6358 (1995).
- [34] A. K. Pant, D. W. J. Cruikshank, *Acta Crystallographica* **B 24**, 13 (1968).

- [35] B. Vessal, G. N. Greaves, P. T. Martin, A. V. Chadwick, R. Mole, S. Houde-Walter, *Nature* (London) **356**, 504 (1992); W. Smith, G. N. Greaves, M. J. Gillan, *J. Chem. Phys.* **103**, 3091 (1995).
- [36] C. Huang, A. N. Cormack, *J. Chem. Phys.* **93**, 8180 (1990); C. Huang, A. N. Cormack, *J. Chem. Phys.* **95**, 3634 (1991); C. Huang, A. N. Cormack, *J. Mater. Chem.* **2**, 281 (1992).
- [37] G. N. Greaves, *Solid State Ionics* **105**, 243 (1998).
- [38] I. Farnam, P. J. Grandinetti, J. H. Baltisberger, J. F. Stebbins, U. Werner, M. Eastman, M. Pines, *Nature* (London) **358**, 21 (1992).
- [39] P. Zhang, P. J. Grandinetti, J. F. Stebbins, *J. Phys. Chem. B* **107**, 4004 (1997).
- [40] K. Glock, O. Hirsch, P. Rehak, B. Thomas, J. Jäger, *J. Non-Cryst. Solids* **232**, 113 (1998).
- [41] R. McGreevy, *J. Non-Cryst. Solids* (in press 2000).
- [42] A. C. Wright, A. G. Clare, B. Bachra, R. N. Sinclair, A. C. Hannon, B. Vessal, *Trans. Amer. Cryst. Assoc.* **27**, 239 (1991).
- [43] W. Smith, G. N. Greaves, M. J. Gillan, *J. Non-Cryst. Solids* **192-193**, 267 (1995).
- [44] G. N. Greaves, W. Smith, E. Giulotto, E. Pantos, *J. Non-Cryst. Solids* **222**, 13 (1997).
- [45] G. N. Greaves, Y. Vaills, S. Sen, unpublished results.
- [46] M. Jermy, Ph. D. Thesis, University of Kent at Canterbury, (1996).
- [47] G. Beaucage, T. A. Ulibarri, E. P. Black, D. W. Schaefer in *Hybrid Organics-Inorganic Composites*, American Chemical Society, 97 (1995).
- [48] R. L. Mozzi, B. E. Warren, *J. Appl. Cryst.* **2**, 164–172 (1969).
- [49] R. J. Bell, P. Dean, *Phil. Mag.* **25**, 1381-1398 (1972).
- [50] F. Gladden, *J. Non-Cryst. Solids*, **119**, 318-330 (1990).
- [51] B. Vessal, M. Amini, C. R. A. Catlow, *J. Non-Cryst. Solids* **159**, 184-186 (1993).
- [52] A. Nakano, R. K. Kalia, P. Vashishta, *J. Non-Cryst. Solids* **171**, 157 (1994).
- [53] S. R. Elliott, *J. Non-Cryst. Solids* **182**, 40 (1995).
- [54] S. R. Elliott, *Phys. Rev. Lett.* **67**, 711 (1991); S. R. Elliott, *J. Phys.: Condens. Matter* **4**, 7661 (1992).
- [55] P. S. Salmon, *Proc. Roy. Soc. (London)* **A 445**, 351 (1994).
- [56] M. Misawa, D. L. Price, K. Suzuki, *J. Non-Cryst. Solids* **37**, 85 (1980).
- [57] F. Meneau, G. N. Greaves, R. Winter, *J. Non-Cryst. Solids* (in press 2000).
- [58] J. Diximier, *J. Phys. I (Paris)* **2**, 1011 (1992).
- [59] M. Wilson, P. A. Madden, *Phys. Rev. Lett.* **72**, 3033 (1994).
- [60] H. Tatlipiari, Z. Akdeniz, G. Pastore, M. P. Tosi, *J. Phys: Cond. Matter* **4**, 8933 (1992).
- [61] S. Susman, K. J. Volin, D. G. Montague, D. C. Price, *Phys. Rev.* **B 43**, 11076 (1991).